JBC RESEARCH ARTICLE

ATP synthesis of *Enterococcus hirae* V-ATPase driven by sodium motive force

Received for publication, December 27, 2024, and in revised form, March 4, 2025 Published, Papers in Press, March 19, 2025,
https://doi.org/10.1016/j.jbc.2025.108422

Akihiro Otomo[1,2,*], **Lucy Gao Hui Zhu**[3], **Yasuko Okuni**[1], **Mayuko Yamamoto**[1], **and Ryota Iino**[1,2,*]

From the [1]*Institute for Molecular Sciences, National Institutes of Natural Sciences, Okazaki, Aichi, Japan;* [2]*Graduate Institute for Advanced Studies, SOKENDAI, Kanazawa, Japan;* [3]*Chimie Paris Tech, Paris, France*

Reviewed by members of the JBC Editorial Board. Edited by Enrique De La Cruz

V-ATPases generally function as ion pumps driven by ATP hydrolysis in the cell, but their capability of ATP synthesis remains largely unexplored. Here we show ATP synthesis of Na^+-transporting *Enterococcus hirae* V-ATPase (EhV_oV_1) driven by the electrochemical potential gradient of Na^+ across the membrane (sodium motive force, *smf*). We reconstituted EhV_oV_1 into liposome and performed a luciferin/luciferase-based assay to analyze ATP synthesis quantitatively. Our result demonstrates that EhV_oV_1 synthesizes ATP with a rate of 4.7 s^{-1} under high *smf* (269.3 mV). The Michaelis constants for ADP (21 μM) and inorganic phosphate (2.1 mM) in ATP synthesis reaction were comparable to those for ATP synthases, suggesting similar substrate affinities among rotary ATPases regardless of their physiological functions. Both components of *smf*, Na^+ concentration gradient across the membrane (ΔpNa) and membrane potential (Δψ), contributed to ATP synthesis, with ΔpNa showing a slightly larger impact. At the equilibrium points where *smf* and Gibbs free energy of ATP synthesis are balanced, EhV_oV_1 showed reversible reactions between ATP synthesis and hydrolysis. The obtained Na^+/ATP ratio (3.2 ± 0.4) closely matched the value expected from the structural symmetry ratio between EhV_o and EhV_1 (10/3 = 3.3), indicating tight coupling between ATP synthesis/hydrolysis and Na^+ transport. These results reveal the inherent functional reversibility of EhV_oV_1. We propose that the physiological function of EhV_oV_1 *in vivo* is determined by relatively small *smf* against large Gibbs free energy of ATP synthesis, in addition to the absence of inhibitory mechanisms of ATP hydrolysis which are known for ATP synthases.

F-, V-, and A-ATPases (F_oF_1, V_oV_1, and A_oA_1, respectively) are rotary motor proteins and are classified together as rotary ATPases (1–4). These rotary ATPases share a common structural architecture: a cytoplasmic domain (F_1, V_1 or A_1) for ATP synthesis and hydrolysis and a membrane-embedded domain (F_o, V_o, or A_o) for the transport of proton (H^+) or sodium ion (Na^+). F-ATPases are present in mitochondria and chloroplasts of eukaryotes and plasma membranes of many bacteria, and primarily function as ATP synthases. ATP synthesis reaction is driven by the ion motive force (*imf*), the electrochemical potential gradient of the ion across the membrane, generated by respiratory chains or photosynthesis. F-ATPases show reversible energy conversion, being capable of pumping H^+ or Na^+ by hydrolyzing ATP when the *imf* is insufficient and/or the ATP/ADP ratio is high in the cell (1).

V-ATPases are located in eukaryotic organelles and some bacterial plasma membranes and generally operate as ATP hydrolysis-driven ion pumps (5, 6). Bacterial V-ATPases typically consist of A, B, D, E, F, and G subunits in V_1 and a, c, and d subunits in V_o with some exceptions, and eukaryotic V-ATPases often have additional, organism-specific subunits and isoforms (7, 8). V-ATPases play crucial roles in organelle acidification, homeostasis of H^+ or Na^+ concentration in the cell, and other cellular processes (9, 10). Interestingly, the V/A-ATPase from *Thermus thermophilus* (TtV_oV_1) functions as an ATP synthase in the cell, in contrast to other V-ATPases (11, 12). Archaea possess A-ATPases structurally similar to V-ATPases but primarily function as ATP synthases, highlighting the diverse roles of these rotary ATPases across life domains (3, 4).

ATP synthesis catalyzed by rotary ATPases has been mostly studied with F- and A- ATPases and TtV_oV_1, all of which physiologically function as ATP synthases (13–20). Very few studies have been conducted with V-ATPases, so our understanding of their potential reversibility is very limited (4, 21). Hirata *et al.* provided the first evidence for ATP synthesis of V-ATPase from *Saccharomyces cerevisiae* (ScV_oV_1) in vacuolar membrane driven by the *imf* generated by a pyrophosphatase. They observed biphasic kinetics with two Michaelis constants (K_m) for ADP of 6.9 and 29 μM, with corresponding maximum velocities of 2.9 and 4.9 nmol mg^{-1} min^{-1}, respectively (Table 1) (22). However, for V-ATPases, important parameters for reversibility remain unexplored, such as equilibrium points between ATP synthesis and hydrolysis, and ion/ATP coupling ratio between V_o and V_1.

The ion/ATP coupling ratio is one of the most crucial parameters for rotary ATPases, which determines the equilibrium points and directions of their operations, ATP synthesis, or hydrolysis (14). This ratio represents the number of ions transported per ATP molecule synthesized or hydrolyzed. The

* For correspondence: Akihiro Otomo, otomoa@ims.ac.jp; Ryota Iino, iino@ims.ac.jp.
Present address for Akihiro Otomo: Department of Chemistry, Graduate School of Science, Kyoto University, Kitashirakawa-Oiwakecho, Sakyo-ku, Kyoto, 606–8502, Japan.

Table 1
Kinetic parameters for ATP synthesis of EhV_oV_1 and other rotary ATPases

Enzyme[a]	$K_{m,\ ADP}$ (μM)	$K_{m,\ Pi}$ (mM)	k_{cat} (s^{-1})	Ion motive force (mV)	Temperature (°C)	References
EhV_oV_1	21 ± 2	2.1 ± 0.2	4.7	269	25	This study
EF_oF_1 WT	100 ± 12	4.2 ± 0.92	16–20	264	24–25	(17)
EF_oF_1 εΔC[b]	25 ± 5.8	3.2 ± 0.86	55–66	264	24–25	(17)
EF_oF_1 WT	27	0.7	∼30	330	R.T.	(20)
TF_oF_1 WT	-	-	<1	330	30	(18)
TF_oF_1 εΔC[b]	13	0.55	∼15	330	30	(18)
TtV_oV_1	5.4 ± 1.3	0.3 ± 0.09	35–45	290	25	(19)
ScV_oV_1[c]	6.9, 29[d]	-	2.9, 4.9[d] (nmol mg^{-1} min^{-1})[e]	-	10	(22)

[a] EhV_oV_1, V_oV_1 from *Enterococcus hirae*; EF_oF_1, F_oF_1 from *Escherichia coli*; TF_oF_1, F_oF_1 from thermophilic *Bacillus* PS3; TtV_oV_1, V/A-ATPase from *Thermus thermophilus*; ScV_oV_1, V_oV_1 from *Saccharomyces cerevisiae*.
[b] Mutant that lacks C-terminal α-helices of the ε subunit.
[c] Vacuolar membranes were used for measurements.
[d] ScV_oV_1 exhibited biphasic kinetics with respect to ADP concentration, although the underlying mechanism remains unclear.
[e] Activity (maximum velocity) was expressed with the unit of nmol mg^{-1} min^{-1}.

rotary catalysis in F_1, V_1, and A_1 accompanies the rotation of the central stalk in the hexameric stator ring. Single rotation is coupled with the synthesis or hydrolysis of 3 ATP molecules, reflecting the three catalytic sites in the hexameric stator ring. The rotation of the central stalk in F_1, V_1, and A_1 is coupled with ion transport through a stator a-subunit and a rotor c-ring of F_o, V_o, and A_o (1, 2). The c-ring, composed of multiple c-subunits each with one ion binding site, determines the number of ions transported per single rotation. The number of c-subunits in a c-ring varies among species (8–17), resulting in an ion/ATP coupling ratio ranging from 2.7 to 5.7 (23). The direction of the chemical reaction, ATP synthesis, or hydrolysis in these enzymes is thermodynamically governed by the relationship between the Gibbs free energy of ATP synthesis and *imf*:

$$\Delta G' = \Delta G^{\circ\prime} + k_B T \cdot \ln K_{(ATP)} - n \cdot imf \quad (1)$$

$$K_{(ATP)} = [ATP]/([ADP] \cdot [Pi]) \quad (2)$$

where $\Delta G^{\circ\prime}$ is the standard Gibbs free energy of ATP synthesis, k_B is the Boltzmann constant, T is absolute temperature, $K_{(ATP)}$ is the ratio of ATP concentration ([ATP]) to ADP and inorganic phosphate (Pi) concentrations ([ADP] and [Pi], respectively), and n is the ion/ATP coupling ratio, respectively. A large n value allows ATP synthesis even at low *imf*, and this value is presumably related to the environments in which living organisms grow (15, 16, 23, 24).

The V-ATPase from *Enterococcus hirae* (EhV_oV_1) is an ion pump that transports Na^+, enabling *E. hirae* to grow in alkaline environments by maintaining Na^+ homeostasis (25, 26). Extensive studies have elucidated the structure of EhV_oV_1 (27–32) and its rotary dynamics driven by ATP hydrolysis (33–36). The EhV_o has a c-ring composed of 10 c-subunits (28). Therefore, the expected Na^+/ATP ratio for EhV_oV_1 is 3.3 (10/3), similar to the H^+/ATP ratio of 3.3 for F-ATPases from *Escherichia coli* (EF_oF_1) (37) and thermophilic *Bacillus* PS3 (TF_oF_1) (38–40). However, no studies have examined whether EhV_oV_1 can synthesize ATP using the sodium motive force (*smf*), composed of the electrochemical potential of Na^+ across the membrane (ΔpNa) and the membrane potential (Δψ).

The present study aims to elucidate the ATP synthesis capability of EhV_oV_1 driven by the *smf*. We reconstituted EhV_oV_1 into liposomes, allowing precise control of the *smf*, and employed a luciferin/luciferase-based assay for ATP detection (Fig. 1). This approach enabled us to demonstrate that EhV_oV_1 can synthesize ATP driven by *smf*. Quantitative analysis revealed [ADP], [Pi], and *smf* dependences of ATP synthesis rate, and kinetic contributions of ΔpNa and Δψ to ATP synthesis. Furthermore, we revealed high thermodynamic efficiency (3.2 Na^+/ATP ratio comparable to the value of 3.3 expected from the structure) of EhV_oV_1 at the equilibrium point between ATP synthesis and hydrolysis, similar to previously studied ATP synthases (13, 41). Our results provide new insights into the inherent functional reversibility of V-ATPases, and raise intriguing questions about the physiological relevance of their ATP synthesis capability; how these rotary ATPases have acquired distinct physiological functions,

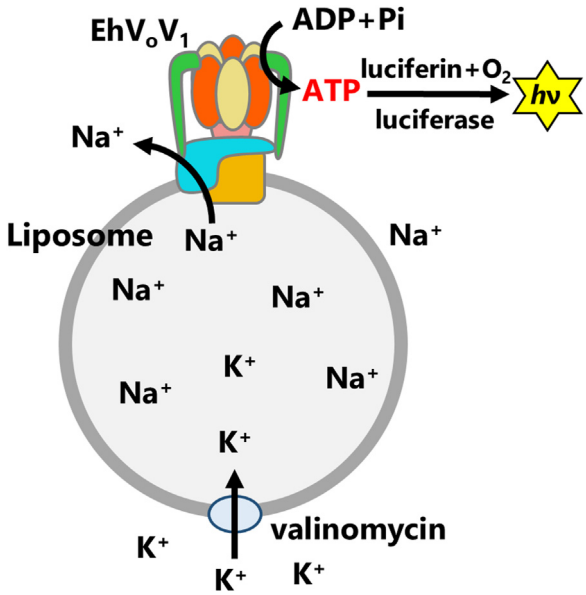

Figure 1. Schematic illustration of ATP synthesis experiment of EhV_oV_1 reconstituted into liposome. ATP synthesis was driven by *smf*, generated by sum of Na^+ concentration gradient (ΔpNa) and K^+-valinomycin diffusion potential (Δψ) across the membrane. Synthesized ATP was detected as luminescence using luciferin/luciferase system.

ATP synthesis and active ion pumping, although these enzymes share similar rotary catalysis.

Results

Demonstration of smf*-driven ATP synthesis of EhV$_o$V$_1$ and its dependence on [ADP] and [Pi]*

The ATP synthesis activity of EhV$_o$V$_1$ reconstituted into liposome was measured *via* the luminescence intensity change of the luciferin/luciferase system at 25 °C (Fig. 1). The linear relationship between luminescence intensity and [ATP] up to 1 μM and the rapid response of the luminescence signal to ATP addition were confirmed (Fig. S1). The imposed *smf* was calculated by the equation:

$$smf = 2.3(k_BT/e)\cdot \Delta pNa + \Delta\psi = 2.3(k_BT/e)\cdot log_{10}\left([Na^+]_{in}/[Na^+]_{out}\right) + 2.3(k_BT/e)\cdot log_{10}\left([K^+]_{out}/[K^+]_{in}\right) \quad (3)$$

where e is the elementary charge, and $[Na^+]_{in}$ and $[Na^+]_{out}$ ($[K^+]_{in}$ and $[K^+]_{out}$) are Na^+ (K^+) concentrations inside and outside the liposome, respectively. The $\Delta\psi$ was applied using K^+-valinomycin diffusion potential. To accurately calculate *smf*, we measured ion concentrations unintendedly contained in the buffers and regents using an inductively coupled plasma optical emission spectrometer (ICP-OES) (Fig. S2). The solution compositions used for measurements in this study are summarized in Tables S1–S3.

Figures 2*A* and S3 show the time courses of ATP synthesis of EhV$_o$V$_1$ under the high *smf* (269.3 mV: $\Delta\psi$ of 154.7 mV and $2.3(k_BT/e)\cdot\Delta$pNa of 114.6 mV) and various [ADP] and [Pi]. Note that to facilitate ATP synthesis, we did not add ATP intentionally but a small amount of ATP was contaminated in ADP (<0.003%) (Table S1). The observed increments in the luminescence intensity after the addition of proteoliposome (PL) indicate that EhV$_o$V$_1$ synthesizes ATP driven by *smf*. The intensity changes were converted into [ATP] changes based on the luminescence increase caused by the addition of 200 nM ATP at the end of each measurement. ATP synthesis rates were estimated by fitting the intensity change after the addition of PL with a single exponential function and calculating the initial slope of the fitted curve.

As a result, [ADP] and [Pi] dependences of the ATP synthesis rates were well fitted by the Michaelis-Menten equation, yielding the same k_{cat} of 4.7 s^{-1} for both [ADP] and [Pi] dependences, and $K_{m,\ ADP}$ = 21 μM and $K_{m,\ Pi}$ = 2.1 mM for [ADP] and [Pi] dependences, respectively (Fig. 2*B*). These K_m values for EhV$_o$V$_1$ were comparable to those of other rotary

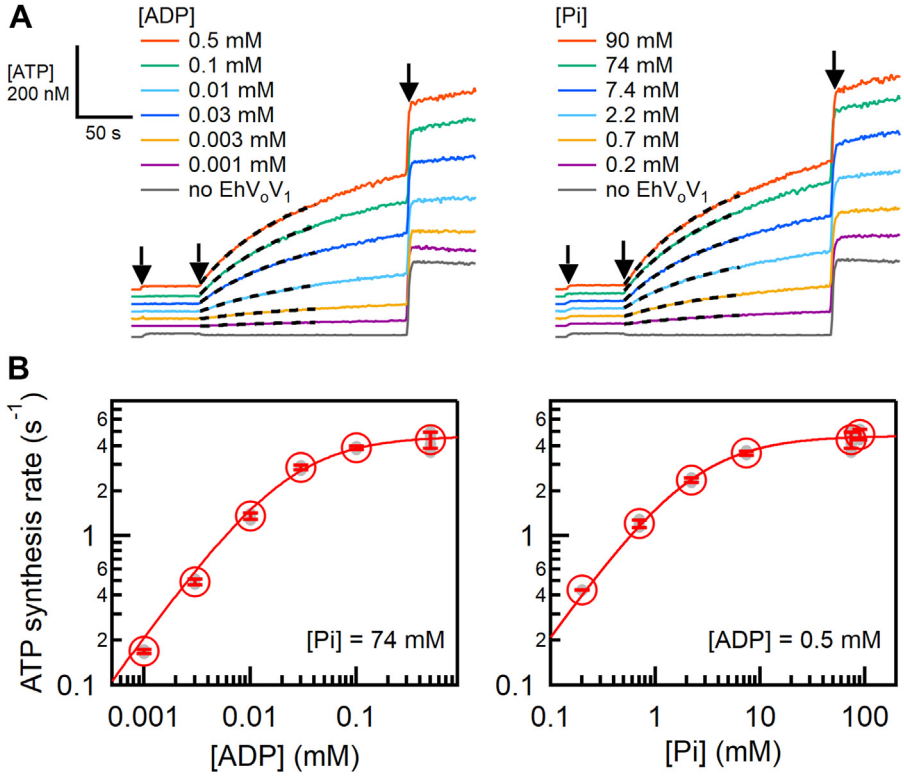

Figure 2. ATP synthesis of EhV$_o$V$_1$ driven by *smf*. *A*, [ADP] (*left*) and [Pi] (*right*) dependences of ATP synthesis activity of EhV$_o$V$_1$ under *smf* of 269.3 mV ($\Delta\psi$ of 154.7 mV and $2.3(k_BT/e)\cdot\Delta$pNa of 114.6 mV). [Pi] (*left*) and [ADP] (*right*) were set at 74 and 0.5 mM, respectively. ATP was not added but contaminated in ADP (<0.003%) (Table S1). ADP (0.001–0.5 mM), proteoliposome (PL) or liposome without EhV$_o$V$_1$ for negative control experiments (*gray traces*), and ATP (200 nM) were added at 10, 60, and 240 s, respectively, as indicated by *black arrows*. The *black dashed lines* represent the fitting with a single exponential function for Δt = 100 s after the addition of PL. The gray traces are negative control experiments using liposome without EhV$_o$V$_1$ at *smf* of 269.3 mV, 74 mM Pi, and 0.5 mM ADP. All traces are shown in Fig. S3. *B*, ATP synthesis rate against [ADP] (*left*) and [Pi] (*right*). *Red open circles* represent mean values obtained from more than three measurements. Individual data points are shown as *gray-filled circles*. Error bars indicate standard deviations. The *red lines* show the fitting with the Michaelis-Menten equation.

ATPases that function as ATP synthases physiologically (Table 1). The comparable values of K_m suggest that the affinities of ADP and Pi in ATP synthesis reaction are similar across EhV$_o$V$_1$ and these enzymes regardless of their primary physiological functions.

Kinetic contributions of ΔpNa and Δψ to ATP synthesis

We next investigated the contributions of Δψ and ΔpNa to the ATP synthesis rate of EhV$_o$V$_1$ by changing the ΔpNa or Δψ under constant Δψ (77.0 or 78.0 mV) or 2.3(k_BT/e) · ΔpNa (76.5 or 76.9 mV), respectively (Fig. 3*A*, left and right, respectively and Fig. S4). The experiment was designed to compare the impacts of Δψ and ΔpNa under nearly equivalent total *smf* values ranging from ∼77 to ∼150 mV. In this series of experiments, [ADP] and [Pi] were set at 0.5 mM and 25 mM, respectively. Again, to facilitate ATP synthesis, we did not add ATP intentionally but a small amount of ATP was contaminated in ADP (<0.003%) (Table S2).

As a result, ATP synthesis was not detected at the lowest *smf* values, 2.3(k_BT/e) · ΔpNa of 78.0 mV or Δψ of 76.5 mV alone (Fig. 3*A*, bottom). However, once the total *smf* exceeded these values, ATP synthesis was observed, indicating that the threshold *smf* for ATP synthesis lies in this range. As the *smf* increased, the ATP synthesis rate increased, regardless of whether Δψ or ΔpNa increased. Figure 3*B* shows the Δψ (red) and ΔpNa (blue) dependences of the ATP synthesis rate. Although ΔpNa exhibited a slightly larger impact than Δψ, the ATP synthesis rate increased as Δψ or ΔpNa increased, suggesting nearly equivalent kinetic contributions of Δψ and ΔpNa to the ATP synthesis of EhV$_o$V$_1$.

Thermodynamic efficiency at the equilibrium points between ATP synthesis and hydrolysis

We then investigated the equilibrium points where ATP synthesis and hydrolysis are balanced. According to Equations 1 and 2, the direction of ATP synthesis/hydrolysis reaction is determined by the magnitudes of $K_{(ATP)}$ and *smf*. To determine the equilibrium points under various $K_{(ATP)}$ and *smf* conditions, we conducted experiments with ATP at 25 nM, Pi at 9.95 mM, and ADP varying from 10 to 80 μM, under *smf* conditions ranging from 93.5 to 132.6 mV (Table S3). Figure 4, *A–D*, and Fig. S5 show the time courses of the luminescence intensity or [ATP] under these conditions. We observed ATP synthesis at high *smf* and ATP hydrolysis at low *smf*, as indicated by positive and negative slopes, respectively.

The calculated catalysis rates were plotted against *smf* (Fig. 4, *E–H*). The positive and negative values correspond to ATP synthesis and hydrolysis rates, respectively. At low *smf*, EhV$_o$V$_1$ showed nearly constant ATP hydrolysis rates, presumably because ATP binding is the rate-limiting at 25 nM ATP. At high *smf*, EhV$_o$V$_1$ showed *smf*-dependent changes in the rates from ATP hydrolysis to synthesis. Then, we determined smf_{eq} (*smf* at which the net rate of ATP synthesis/hydrolysis is zero, black arrows) by linearly interpolating the two data points crossing the catalysis rate of zero. At this equilibrium point, Δ*G*' in Equation 1 is zero and Equation 1 can be transformed into the following equation:

$$k_BT \cdot \ln K_{(ATP)eq} = -\Delta G^{o\prime} + n \cdot smf_{eq} \quad (4)$$

where $K_{(ATP)eq}$ is the ratio of [ATP] to [ADP][Pi] at the equilibrium point. Based on Equation 4, $k_BT \cdot \ln K_{(ATP)eq}$ was plotted as a function of smf_{eq} (Fig. 5) and fitted with a linear function.

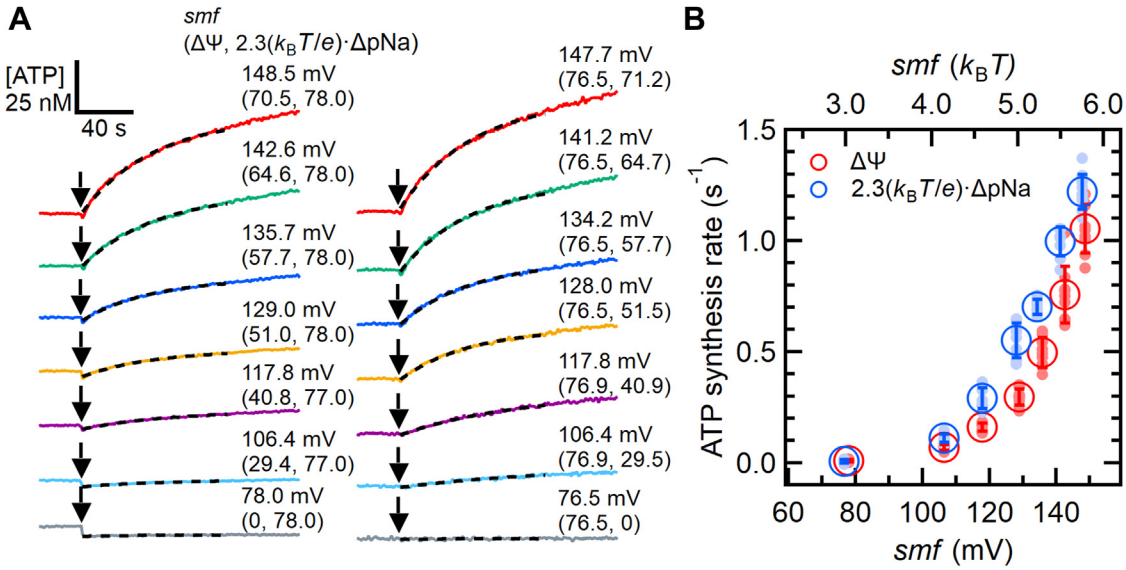

Figure 3. Contribution of Δψ and ΔpNa to ATP synthesis of EhV$_o$V$_1$. *A*, enlarged view of typical time courses of ATP synthesis at different *smf*. The entire time courses of all traces are shown in Fig. S4. The reaction was initiated by adding proteoliposome (PL) (*black arrows*). [Pi] and [ADP] were 25 and 0.5 mM, respectively. ATP was not added but contaminated in ADP (<0.003%) (Table S2). In the left panel, Δψ was varied from 0 to 70.5 mV under 2.3(k_BT/e)·ΔpNa of 77.0 or 78.0 mV. In the *right panel*, 2.3(k_BT/e)·ΔpNa was varied from 0 to 71.2 mV under Δψ of 76.5 or 76.9 mV. The *black dashed lines* represent the fitting with a single exponential function for Δt = 100 s after the addition of PL. *B*, Δψ (*red*) and 2.3(k_BT/e)·ΔpNa (*blue*) dependences of ATP synthesis rate. Closed and open circles represent the individual measurements (N ≥ 8) and mean values, respectively. Error bars indicate standard deviations.

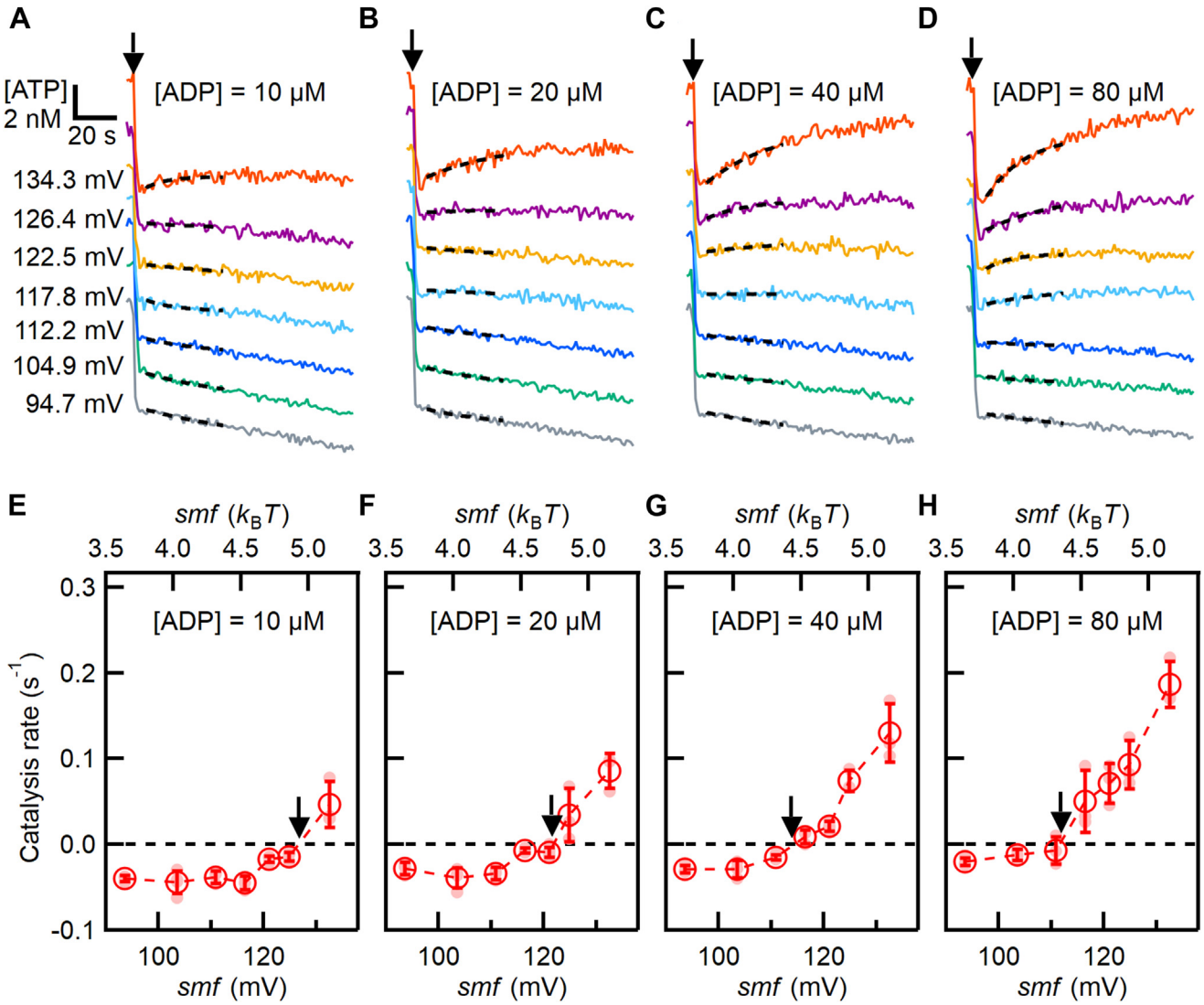

Figure 4. Determination of the equilibrium points between ATP synthesis and hydrolysis. *A–D*, typical time courses of ATP synthesis and hydrolysis at different *smf* (93.5–132.6 mV). Reaction was initiated by adding proteoliposome (PL) as indicated by *black arrow*. The *black dashed lines* represent the fitting with a single exponential function for Δt = 35 s after the addition of PL. The entire time courses of all traces are shown in Fig. S5. *E–H*, *smf* dependence of ATP synthesis and hydrolysis rates. *Black arrows* indicate equilibrium points obtained by linear fitting between two data points across the catalysis rate of zero. The reaction solution contains 25 nM ATP, 9.95 mM Pi, and ADP at 10 μM (*A* and *E*), 20 μM (*B* and *F*), 40 μM (*C* and *G*), and 80 μM (D and *H*), respectively (Table S3).

The slope and y-intercept of the fitted line correspond to the ion/ATP ratio n and the standard Gibbs free energy of ATP synthesis $\Delta G^{\circ\prime}$, respectively, and n of 3.2 ± 0.4 (fitted value ± SE of the fit) and $\Delta G^{\circ\prime}$ of 17.0 ± 1.7 k_BT (42.2 ± 4.2 kJ/mol) were obtained. The value of the $\Delta G^{\circ\prime}$ was similar to those (36 ∼ 39 kJ/mol) previously reported for other ATP synthases (13, 41–43), validating our experimental system. The experimentally determined value of the n (3.2) showed excellent agreement with that (10/3 = 3.3) expected from the structural composition of EhV_oV_1 which has 3 ATP catalytic sites in EhV_1 and 10 Na^+ binding sites in the c-ring of EhV_o (27–32).

Discussion

The present study demonstrated that EhV_oV_1 is capable of synthesizing ATP driven by *smf*, despite its physiological function as an ATP-driven Na^+ pump. The obtained values of the K_m for ADP (21 μM) and Pi (2.1 mM) during ATP synthesis of EhV_oV_1 are comparable to those of other ATP synthases (Table 1). The comparable values of K_m indicate similar substrate affinities during ATP synthesis across different rotary ATPases, irrespective of their primary physiological functions. The conserved properties of kinetic parameters may reflect a common evolutionary origin of these rotary ATPases (44, 45).

On the other hand, the observed k_{cat} for EhV_oV_1 is lower than those for other ATP synthases (Table 1). As the K_m values reflect substrate affinity, the low ATP synthesis rate might be caused by a low product (ATP) release rate. Furthermore, previous single-molecule and biochemical studies revealed that at high [ATP], EhV_oV_1 also shows lower ATP hydrolysis rates (120 s^{-1} in single-molecule study using low-load probe (35) and 177 s^{-1} in biochemical assay (36)) compared to F-type

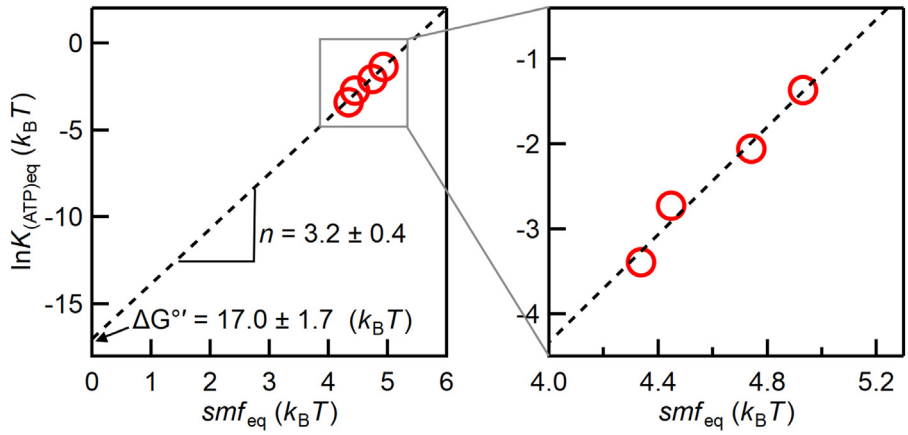

Figure 5. Relationship between k_BT·ln$K_{(ATP)eq}$ and smf_{eq} at the equilibrium points. The *dashed line* shows the fitting with a linear function. The slope and extrapolated y-intercept indicate the Na^+/ATP ratio n (3.2 ± 0.4, fitted value ± S.E. of fitting) and the standard Gibbs free energy of ATP synthesis $\Delta G^{\circ\prime}$ (17.0 ± 1.7 k_BT or 42.0 ± 4.2 kJ/mol), respectively.

ATP synthases such as TF_oF_1 (1056 s^{-1} in single-molecule study using low-load probe (46)) and EF_oF_1 (285 s^{-1} in biochemical assay (17)). These findings may indicate low rates of ATP cleavage/ADP-Pi bond formation process and/or Na^+ transport for EhV$_o$V$_1$ (35). To better understand these kinetic differences, a detailed single-molecule analysis of rotary ATPases during ATP synthesis, which has not yet been fully achieved, is required.

The relatively low K_m value for Pi (high affinity of Pi) during ATP synthesis of EhV$_o$V$_1$ comparable to other ATP synthases is noteworthy (Table 1). Our previous single-molecule study on isolated EhV$_1$ revealed a low affinity of Pi and a chemo-mechanical coupling scheme during rotation driven by ATP hydrolysis (34). In this scheme, Pi is released immediately after the hydrolysis of ATP into ADP and Pi without rotation, followed by the release of ADP after 40° rotation. The low affinity of Pi for EhV$_1$ is also supported by structural studies and MD simulation (28, 47). In contrast, F_1 isolated from thermophilic *Bacillus* PS3 F_oF_1 (TF_1), which physiologically functions as an ATP synthase, exhibits the opposite order of product release during ATP-driven rotation in which ADP is released first and Pi is released second at the different rotation angles (48). This order in TF_1 has been proposed to be favorable for ATP synthesis under physiological high [ATP] and low [ADP] environments, because Pi bound to the catalytic site would prevent ATP binding and facilitate ADP binding. Our current results with EhV$_o$V$_1$ suggest that the order of ADP and Pi release (or the order of ADP and Pi binding in ATP synthesis reaction) itself is not critical for the ATP synthesis capability of rotary ATPases. Our results also suggest dynamic modulation of the substrate (product) affinity depending on the rotation angle and direction, as demonstrated with TF_1 (49). Further studies of various rotary ATPases would reveal how they have acquired functional diversity during their evolution.

In EhV$_o$V$_1$, both ΔpNa and Δψ contribute to driving ATP synthesis, with ΔpNa having a slightly larger contribution (Fig. 3). This property is similar to Na^+-transporting A-ATPases from *Eubacterium callanderi* and *Acerobacterium woodii* and H^+-transporting TF_oF_1 (50, 51). In contrast, reports on H^+-transporting EF_oF_1 and Na^+ -transporting *Propionigenium modestum* F_oF_1 suggest that only one component effectively acts as the driving force (17, 50). The difference in kinetic contribution appears to be a specific feature of each rotary ATPase, independent of transporting ion species or physiological functions. Further structural studies during ATP synthesis under precisely controlled ΔpNa (or ΔpH) and Δψ are necessary to understand why these rotary ATPases show different ΔpNa (or ΔpH) and Δψ dependences. Meanwhile, because other factors such as lipid composition of the liposome and buffer and salt compositions of the assay solution may affect their ATP synthesis activities (50, 52), the results of *in vitro* experiments should be carefully interpreted considering their physiological environments.

The nearly identical Na^+/ATP ratios between experimental value (3.2, Fig. 5) and structural prediction (3.3) provide evidence for tight coupling between ATP synthesis/hydrolysis and Na^+ transport in EhV$_o$V$_1$, consistent with our previous single-molecule study of ATP-driven rotation of EhV$_o$V$_1$ rate-limited by Na^+ transport (35). In other words, EhV$_o$V$_1$ operates with high thermodynamic efficiency at the equilibrium point, with minimal energy loss or uncoupling. Similar excellent agreements in ion/ATP ratios have been reported for TtV$_o$V$_1$ and TF_oF_1 (13, 41), suggesting that tight coupling between ATP synthesis/hydrolysis and ion transport is a fundamental feature of rotary ATPases regardless of their physiological functions.

On the other hand, several studies have reported significant differences in the ion/ATP ratios between biochemical experiments and structural predictions for ATP synthases from chloroplast, *E. coli*, and yeast (42, 43). This apparent discrepancy may reflect the different mechanisms among different rotary ATPases or may stem from the difficulties of accurately controlling the *imf*. Factors such as unintended ion contaminations and/or ion leakages across the lipid membrane would affect the results. The use of Na^+, which exhibits significantly lower membrane permeability than H^+ (53), has the advantage of controlling the *imf* precisely.

Despite the ATP synthesis capability of EhV_oV_1 demonstrated *in vitro*, the physiological function appears to be limited to ATP-driven Na^+ pumping *in vivo*. In the intestines where [Na^+] is ∼100 mM (54, 55), *E. hirae* usually maintains Na^+ homeostasis (∼10 mM intracellular concentration) using H^+/Na^+ antiporters driven by the proton motive force (*pmf*) (56, 57). When pH in the intestine increases and *pmf* generation becomes insufficient, EhV_oV_1 expression is induced to pump out Na^+ using ATP hydrolysis instead of the H^+/Na^+ antiporters. Considering the relatively low ΔpNa of ∼1 ($\log_{10}$[100 mM/10 mM]) and high intracellular [ATP] at the millimolar level, ATP synthesis of EhV_oV_1 would be thermodynamically unfavorable (58). Furthermore, interestingly, EhV_oV_1 does not have any known regulatory mechanisms that inhibit ATP hydrolysis such as ADP-Mg^{2+} inhibition (59, 60), subunit-specific inhibition (61–65), inhibition by endogenous regulatory peptide (66–68), reversible disassembly of V_1 and V_o (9, 69, 70), which are commonly found in many ATP synthases and V-ATPases. Therefore, EhV_oV_1 is likely specialized as an ATP-driven Na^+ pump rather than ATP synthase *in vivo*.

Experimental procedures

Expression and purification of EhV_oV_1

The expression and purification of EhV_oV_1 were performed according to a previously described method (35, 36). Briefly, inverted membranes prepared from *E. coli* (C41(DE3)) expressing EhV_oV_1 with histidine tags in the c-subunits were solubilized using 2% *n*-dodecyl β-$_D$-maltoside (DDM). The solubilized suspension was then applied to a nickel-nitrilotriacetic acid agarose (Ni-NTA agarose, QIAGEN) column. The EhV_oV_1 complex was eluted using a buffer containing 50 mM potassium phosphate (pH7.0), 5 mM $MgCl_2$, 100 mM NaCl, 10% glycerol, and 0.05% DDM. After the elution, the complex was concentrated and subjected to size-exclusion chromatography using Supderdex 200 Increase 10/300 column (Cytiva). The column was equilibrated with a buffer containing 50 mM Tris-HCl (pH7.5), 5 mM $MgCl_2$, 50 mM NaCl, 10% glycerol, and 0.05% DDM. The chromatography was performed using a fast protein liquid chromatography system (Äkta go GE Healthcare) at 4 °C. The purified EhV_oV_1 was concentrated to approximately 20 μM and stored at −80 °C until use.

Reconstitution of EhV_oV_1 into liposome

L-α-Phosphatidylcholine from soybean (Type II-S, Sigma-Aldrich) was washed with acetone and suspended in reconstitution buffer (100 mM BisTris (pH7.0) containing 5 mM $MgCl_2$ and 150 mM sucrose, and specific concentrations of NaCl and KCl described in Table S1-S3) at 40 mg/ml. The suspension underwent three freeze-thaw cycles. After ultracentrifugation (150,000*g* for 90 min at 4 °C), the pellet was resuspended in reconstitution buffer and subjected to another freeze-thaw cycle. This procedure was repeated three times to remove unintended Na^+ and K^+ from the lipids. The liposome was stored at −80 °C until use. Proteoliposome (PL) was prepared by mixing liposome with purified EhV_oV_1 at a volume ratio of 99:1. The mixture was gently mixed by inverting the tube 20 times and subjected to one freeze-thaw cycle. The final concentration of EhV_oV_1 in the PL was 0.2 μM. The prepared PL was stored at −80 °C until use.

Measurement of [Na^+] and [K^+] unintendedly contained in samples

[Na^+] and [K^+] unintendedly contained in the Type II-S lipid and a luciferin/luciferase reagent (ATP bioluminescence assay kit CLS II, Roche) were estimated using inductively coupled plasma optical emission spectrometer (ICP-OES, Agilent Technologies) (Fig. S2). The flow rates of the plasma and assist gas (argon) were 14 and 12 L/min, respectively. The emission intensities were measured at λ = 589.592 and 766.491 nm for sodium and potassium, respectively. Samples were prepared as follows: luciferin/luciferase reagent was dissolved in ultra-pure water (18 mg/ml), Type II-S lipid was suspended in ultra-pure water (40 mg/ml) and liposome was prepared by the above method (40 mg/ml). For calibration, each sample was supplemented with a sodium or potassium standard solution (FUJIFILM Wako). The concentrations of sodium and potassium standard solutions were adjusted between 0.01 and 21.7 mM and between 0.639 and 63.9 mM, respectively, with specific ranges for Type II-S lipid and luciferin/luciferase reagent samples. After the addition of the standard solution, samples were further diluted with ultra-pure water to bring them within the calibration range, and the final concentrations were calculated considering the dilution factors. Each measurement was performed in triplicate, and the average values were used for analysis.

Hexokinase treatment of ADP

Commercial ADP (117,105, Merck) was treated with hexokinase (H4502, Sigma) to reduce ATP contamination as described in a previous study (17). Briefly, 970 μl of ADP solution (∼200 mM) was incubated with 1.3 mg hexokinase, 20 mM glucose, and 5 mM $MgSO_4$ at 25 °C for 30 min. ADP was then purified by gel filtration (NAP10, Cytiva) and stored at −80 °C until use. The treated ADP was used for all ATP synthesis measurements.

Measurement of ATP synthesis/hydrolysis activity

ATP synthesis and hydrolysis activities of EhV_oV_1 reconstituted into liposome were measured using a luminometer (AB-2270, ATTO) and the luciferin/luciferase reagent (ATP bioluminescence assay kit CLS II, Roche). ATP-dependent light emission from luciferin catalyzed by luciferase was monitored (13, 17, 18). The reaction mixture was prepared in a 1.5 ml tube containing 890 μl of observation buffer (100 mM BisTris (pH7.0) containing 5 mM $MgCl_2$ and 150 mM sucrose, and specific concentrations of NaCl, KCl, and phosphate as detailed in Tables S1–S3), 10 μl of valinomycin (final concentration: 83 nM), and 100 μl of luciferin/luciferase reagent (final concentration: 1.5 mg/ml). The tube was placed in the luminometer, and the measurement was initiated. At 10 s,

100 μl of hexokinase-treated ADP was added at the desired concentration, ranging from 0.001 to 0.5 mM. At 60 s, 100 μl of PL sample was introduced. The PL sample was prepared immediately before the measurement by mixing 5 μl of PL suspension with 95 μl of observation buffer, resulting in a 20-fold dilution. Finally, at 240 s, 100 μl of ATP (final concentration: 200 nM) was added for calibration. The total measurement time was 300 s.

For experiments determining the equilibrium point of ATP synthesis and hydrolysis reactions, the order and timing of additions were modified as follows. ADP (final concentrations: 10, 20, 40, or 80 μM) was added at 10 s, ATP (final concentration: 25 nM) at 60 s, and the diluted PL sample at 100 s. The total measurement time for these experiments was 200 s.

The rate of ATP synthesis/hydrolysis was determined by fitting the luminescence intensity change after the addition of PL with a single exponential function and calculating the initial slope of the fitted curve. All measurements were performed in more than triplicate at 25 °C.

The *smf* for each experimental condition was calculated by considering both the intentionally added [Na^+] and [K^+] and the unintended contamination of these ions in the Type II-S lipid and a luciferin/luciferase reagent, as measured by ICP-OES. This approach ensured accurate quantification of the actual *smf*.

Data availability

All data supporting this work are available from the corresponding authors upon reasonable request.

Supporting information—This article contains supporting information.

Acknowledgments—We would like to thank Dr Takeshi Murata and Dr Takanori Harashima for their helpful discussions. A part of this work was performed with the aid of Instrument Center, Institute for Molecular Science.

Author contributions—A. O. writing–original draft; A. O. and R. I. visualization; A. O., L. G. H. Z., M. Y., and R. I. validation; A. O. and R. I. supervision; A. O., Y. O., and M. Y.resources; A. O. and R. I. project administration; A. O. and R. I. methodology; A. O., L. G. H. Z., and M. Y. investigation; A. O. and R. I. funding acquisition; A. O. formal analysis; A. O. data curation; A. O. and R. I. conceptualization; R. I. writing–review & editing.

Funding and additional information—This work was supported by JSPS KAKENHI, Japan Society for the Promotion of Science Grants-in-Aid for Scientific Research (JP18H0524, JP21H02454, and JP24K01996 to R. I., JP21K15060 and JP24K17026 to A. O.) and in part by Tatematsu Foundation to A. O.

Conflict of interest—The authors declare that they have no conflicts of interest with the contents of this article.

Abbreviations—The abbreviations used are: ADP, adenosine diphosphate; ATP, adenosine triphosphate; EF_oF_1, F_oF_1 from *Escherichia coli*; *E. hirae*, *Enterococcus hirae*; EhV_oV_1, V_oV_1 from *Enterococcus hirae*; imf, ion motive force; Pi, inorganic phosphate; pmf, proton motive force; PL, proteoliposome; smf, sodium motive force; ScV_oV_1, V_oV_1 from *Saccharomyces cerevisiae*; TF_oF_1, F_oF_1 from thermophilic *Bacillus* PS3; TtV_oV_1, V/A-ATPase from *Thermus thermophilus*.

References

1. Junge, W., and Nelson, N. (2015) ATP synthase. *Annu. Rev. Biochem.* **84**, 631–657
2. Walker, John E. (2013) The ATP synthase: the understood, the uncertain and the unknown. *Biochem. Soc. Trans.* **41**, 1–16
3. Zubareva, V. M., Lapashina, A. S., Shugaeva, T. E., Litvin, A. V., and Feniouk, B. A. (2020) Rotary ion-translocating ATPases/ATP synthases: diversity, similarities, and differences. *Biochemistry (Moscow)* **85**, 1613–1630
4. Müller, V., and Grüber, G. (2003) ATP synthases: structure, function and evolution of unique energy converters. *Cell Mol. Life Sci.* **60**, 474–494
5. Breton, S., and Brown, D. (2013) Regulation of luminal acidification by the V-ATPase. *Physiology* **28**, 318–329
6. Cipriano, D. J., Wang, Y., Bond, S., Hinton, A., Jefferies, K. C., Qi, J., *et al.* (2008) Structure and regulation of the vacuolar ATPases. *Biochim. Biophys. Acta* **1777**, 599–604
7. Vasanthakumar, T., and Rubinstein, J. L. (2020) Structure and roles of V-type ATPases. *Trends Biochem. Sci.* **45**, 295–307
8. Murata, T., Yamato, I., and Kakinuma, Y. (2005) Structure and mechanism of vacuolar Na+-Translocating ATPase from Enterococcus hirae. *J. Bioenerg. Biomembr.* **37**, 411–413
9. Collins, M. P., and Forgac, M. (2020) Regulation and function of V-ATPases in physiology and disease. *Biochim. Biophys. Acta* **1862**, 183341
10. Khan, M. M., and Wilkens, S. (2024) Molecular mechanism of Oxr1p mediated disassembly of yeast V-ATPase. *EMBO Rep.* **25**, 2323–2347
11. Yokoyama, K., and Imamura, H. (2005) Rotation, structure, and classification of prokaryotic V-ATPase. *J. Bioenerg. Biomembr.* **37**, 405–410
12. Yokoyama, K., Oshima, T., and Yoshida, M. (1990) *Thermus thermophilus* membrane-associated ATPase. Indication of a eubacterial V-type ATPase. *J. Biol. Chem.* **265**, 21946–21950
13. Toei, M., Gerle, C., Nakano, M., Tani, K., Gyobu, N., Tamakoshi, M., *et al.* (2007) Dodecamer rotor ring defines H^+/ATP ratio for ATP synthesis of prokaryotic V-ATPase from *Thermus thermophilus*. *Proc. Natl. Acad. Sci. U. S. A.* **104**, 20256–20261
14. Turina, P. D. S., and Peter, G. (2003) H^+/ATP ratio of proton transport-coupled ATP synthesis and hydrolysis catalysed by CF_oF_1-liposomes. *EMBO J.* **22**, 418–426
15. Preiss, L., Klyszejko, A. L., Hicks, D. B., Liu, J., Fackelmayer, O. J., Yildiz, Ö., *et al.* (2013) The c-ring stoichiometry of ATP synthase is adapted to cell physiological requirements of alkaliphilic *Bacillus pseudofirmus* OF4. *Proc. Natl. Acad. Sci. U. S. A.* **110**, 7874–7879
16. Pogoryelov, D., Reichen, C., Klyszejko, A. L., Brunisholz, R., Muller, D. J., Dimroth, P., *et al.* (2007) The oligomeric state of c rings from cyanobacterial F-ATP synthases varies from 13 to 15. *J. Bacteriol.* **189**, 5895–5902
17. Iino, R., Hasegawa, R., Tabata, K. V., and Noji, H. (2009) Mechanism of inhibition by C-terminal α-helices of the ϵ subunit of *Escherichia coli* F_oF_1-ATP synthase. *J. Biol. Chem.* **284**, 17457–17464
18. Soga, N., Kinosita, K., Yoshida, M., and Suzuki, T. (2011) Efficient ATP synthesis by thermophilic *Bacillus* F_oF_1-ATP synthase. *FEBS J.* **278**, 2647–2654
19. Kishikawa, J.-I., Nakanishi, A., Furuike, S., Tamakoshi, M., and Yokoyama, K. (2014) Molecular basis of ADP inhibition of vacuolar (V)-type ATPase/synthase. *J. Biol. Chem.* **289**, 403–412
20. Fischer, S., Etzold, C., Turina, P., Deckers-Hebestreit, G., Altendorf, K., and Gräber, P. (1994) ATP synthesis catalyzed by the ATP synthase of *Escherichia coli* reconstituted into liposomes. *Eur. J. Biochem.* **225**, 167–172
21. Kühlbrandt, W., and Davies, K. M. (2016) Rotary ATPases: a new twist to an ancient machine. *Trends Biochem. Sci.* **41**, 106–116

22. Hirata, T., Nakamura, N., Omote, H., Wada, Y., and Futai, M. (2000) Regulation and reversibility of vacuolar H^+-ATPase. *J. Biol. Chem.* **275**, 386–389
23. Cheuk, A., and Meier, T. (2021) Rotor subunits adaptations in ATP synthases from photosynthetic organisms. *Biochem. Soc. Trans.* **49**, 541–550
24. Yamamoto, H., Cheuk, A., Shearman, J., Nixon, P. J., Meier, T., and Shikanai, T. (2023) Impact of engineering the ATP synthase rotor ring on photosynthesis in tobacco chloroplasts. *Plant Physiol.* **192**, 1221–1233
25. Heefner, D. L., and Harold, F. M. (1982) ATP-driven sodium pump in *Streptococcus faecalis*. *Proc. Natl. Acad. Sci. U. S. A.* **79**, 2798–2802
26. Kakinuma, Y., Yamato, I., and Murata, T. (1999) Structure and function of vacuolar Na^+-Translocating ATPase in *Enterococcus hirae*. *J. Bioenerg. Biomembr.* **31**, 7–14
27. Arai, S., Saijo, S., Suzuki, K., Mizutani, K., Kakinuma, Y., Ishizuka-Katsura, Y., *et al.* (2013) Rotation mechanism of *Enterococcus hirae* V_1-ATPase based on asymmetric crystal structures. *Nature* **493**, 703–707
28. Suzuki, K., Mizutani, K., Maruyama, S., Shimono, K., Imai, F. L., Muneyuki, E., *et al.* (2016) Crystal structures of the ATP-binding and ADP-release dwells of the V_1 rotary motor. *Nat. Commun.* **7**, 13235
29. Tsunoda, J., Song, C., Imai, F. L., Takagi, J., Ueno, H., Murata, T., *et al.* (2018) Off-axis rotor in *Enterococcus hirae* V-ATPase visualized by Zernike phase plate single-particle cryo-electron microscopy. *Sci. Rep.* **8**, 15632
30. Burton-Smith, R. N., Song, C., Ueno, H., Murata, T., Iino, R., and Murata, K. (2023) Six states of *Enterococcus hirae* V-type ATPase reveals non-uniform rotor rotation during turnover. *Commun. Biol.* **6**, 755
31. Suzuki, K., Goto, Y., Otomo, A., Shimizu, K., Abe, S., Moriyama, K., *et al.* (2024) Na^+-V-ATPase inhibitor curbs VRE growth and unveils Na^+ pathway structure. *Nat. Struct. Mol. Biol.* https://doi.org/10.1038/s41594-41024-01419-y
32. Murata, T., Yamato, I., Kakinuma, Y., Leslie, A. G. W., and Walker, J. E. (2005) Structure of the rotor of the V-type Na^+-ATPase from *Enterococcus hirae*. *Science* **308**, 654
33. Minagawa, Y., Ueno, H., Hara, M., Ishizuka-Katsura, Y., Ohsawa, N., Terada, T., *et al.* (2013) Basic properties of rotary dynamics of the molecular motor *Enterococcus hirae* V_1-ATPase. *J. Biol. Chem.* **288**, 32700–32707
34. Iida, T., Minagawa, Y., Ueno, H., Kawai, F., Murata, T., and Iino, R. (2019) Single-molecule analysis reveals rotational substeps and chemo-mechanical coupling scheme of *Enterococcus hirae* V_1-ATPase. *J. Biol. Chem.* **294**, 17017–17030
35. Otomo, A., Iida, T., Okuni, Y., Ueno, H., Murata, T., and Iino, R. (2022) Direct observation of stepping rotation of V-ATPase reveals rigid component in coupling between V_o and V_1 motors. *Proc. Natl. Acad. Sci. U. S. A.* **119**, e2210204119
36. Ueno, H., Minagawa, Y., Hara, M., Rahman, S., Yamato, I., Muneyuki, E., *et al.* (2014) Torque generation of *Enterococcus hirae* V-ATPase. *J. Biol. Chem.* **289**, 31212–31223
37. Sobti, M., Smits, C., Wong, A. S., Ishmukhametov, R., Stock, D., Sandin, S., *et al.* (2016) Cryo-EM structures of the autoinhibited *E. coli* ATP synthase in three rotational states. *eLife* **5**, e21598
38. Sobti, M., Walshe, J. L., Wu, D., Ishmukhametov, R., Zeng, Y. C., Robinson, C. V., *et al.* (2020) Cryo-EM structures provide insight into how E. coli F_1F_o ATP synthase accommodates symmetry mismatch. *Nat. Commun.* **11**, 2615
39. Guo, H., Suzuki, T., and Rubinstein, J. L. (2019) Structure of a bacterial ATP synthase. *eLife* **8**. https://doi.org/10.7554/eLife.43128
40. [preprint] Ueno, H., Yasuda, K., Hamaguchi-Suzuki, N., Marui, R., Adachi, N., Senda, T., *et al.* (2024) Engineering of ATP synthase for enhancement of proton-to-ATP ratio. *bioRxiv*. https://doi.org/10.1101/2024.08.27.609901
41. Soga, N., Kimura, K., Kinosita, K., Yoshida, M., and Suzuki, T. (2017) Perfect chemomechanical coupling of F_oF_1-ATP synthase. *Proc. Natl. Acad. Sci. U. S. A.* **114**, 4960–4965
42. Steigmiller, S., Turina, P., and Gräber, P. (2008) The thermodynamic H^+/ATP ratios of the H^+-ATPsynthases from chloroplasts and *Escherichia coli*. *Proc. Natl. Acad. Sci. U. S. A.* **105**, 3745–3750
43. Petersen, J., Förster, K., Turina, P., and Gräber, P. (2012) Comparison of the H^+/ATP ratios of the H^+-ATP synthases from yeast and from chloroplast. *Proc. Natl. Acad. Sci. U. S. A.* **109**, 11150–11155
44. Gogarten, J. P., Kibak, H., Dittrich, P., Taiz, L., Bowman, E. J., Bowman, B. J., *et al.* (1989) Evolution of the vacuolar H^+-ATPase: implications for the origin of eukaryotes. *Proc. Natl. Acad. Sci. U. S. A.* **86**, 6661–6665
45. Mahendrarajah, T. A., Moody, E. R. R., Schrempf, D., Szánthó, L. L., Dombrowski, N., Davín, A. A., *et al.* (2023) ATP synthase evolution on a cross-braced dated tree of life. *Nat. Commun.* **14**, 7456
46. Ueno, H., Suzuki, T., Kinosita, K., and Yoshida, M. (2005) ATP-driven stepwise rotation of F_oF_1-ATP synthase. *Proc. Natl. Acad. Sci. U. S. A.* **102**, 1333
47. Shekhar, M., Gupta, C., Suzuki, K., Chan, C. K., Murata, T., and Singharoy, A. (2022) Revealing a hidden intermediate of rotatory catalysis with X-ray crystallography and molecular simulations. *ACS Cent. Sci.* **8**, 915–925
48. Watanabe, R., Iino, R., and Noji, H. (2010) Phosphate release in F_1-ATPase catalytic cycle follows ADP release. *Nat. Chem. Biol.* **6**, 814–820
49. Watanabe, R., Okuno, D., Sakakihara, S., Shimabukuro, K., Iino, R., Yoshida, M., *et al.* (2012) Mechanical modulation of catalytic power on F_1-ATPase. *Nat. Chem. Biol.* **8**, 86–92
50. Litty, D., and Müller, V. (2022) ATP synthesis in an ancient ATP synthase at low driving forces. *Proc. Natl. Acad. Sci. U. S. A.* **119**, e2201921119
51. Soga, N., Kinosita, K., Yoshida, M., and Suzuki, T. (2012) Kinetic equivalence of transmembrane pH and electrical potential differences in ATP synthesis. *J. Biol. Chem.* **287**, 9633–9639
52. Pitard, B., Richard, P., Duñach, M., and Rigaud, J.-L. (1996) ATP synthesis by the F0F1 ATP synthase from thermophilic Bacillus PS3 reconstituted into liposomes with bacteriorhodopsin. *Eur. J. Biochem.* **235**, 779–788
53. Van De Vossenberg, J. L. C. M., Ubbink-Kok, T., Elferink, M. G. L., Driessen, A. J. M., and Konings, W. N. (1995) Ion permeability of the cytoplasmic membrane limits the maximum growth temperature of bacteria and archaea. *Mol. Microbiol.* **18**, 925–932
54. Lucas, M. L., and Cannon, M. J. (1983) Measurement of sodium ion concentration in the unstirred layer of rat small intestine by polymer Na^+-sensitive electrodes. *Biochim. Biophys. Acta* **730**, 41–48
55. Bucking, C., and Wood, C. M. (2006) Gastrointestinal processing of Na^+, Cl^-, and K^+ during digestion: implications for homeostatic balance in freshwater rainbow trout. *Am. J. Physiol. Regul. Integr. Comp. Physiol.* **291**, R1764–R1772
56. Kawano-Kawada, M., Takahashi, H., Igarashi, K., Murata, T., Yamato, I., Homma, M., *et al.* (2011) Significance of the glutamate-139 Residue of the V-Type Na^+-ATPase NtpK subunit in catalytic turnover linked with salt tolerance of *Enterococcus hirae*. *J. Bacteriol.* **193**, 3657–3661
57. Ikegami, M., Takahashi, H., Igarashi, K., and Kakinuma, Y. (2000) Sodium ATPase and sodium/proton antiporter are not obligatory for sodium homeostasis of *Enterococcus hirae* at acid pH. *Biosci. Biotechnol. Biochem.* **64**, 1088–1092
58. Meyrat, A., and Von Ballmoos, C. (2019) ATP synthesis at physiological nucleotide concentrations. *Sci. Rep.* **9**, 3070
59. Yokoyama, K., Muneyuki, E., Amano, T., Mizutani, S., Yoshida, M., Ishida, M., *et al.* (1998) V-ATPase of *Thermus thermophilus* is inactivated during ATP hydrolysis but can synthesize ATP. *J. Biol. Chem.* **273**, 20504–20510
60. Hirono-Hara, Y., Noji, H., Nishiura, M., Muneyuki, E., Hara, K. Y., Yasuda, R., *et al.* (2001) Pause and rotation of F_1-ATPase during catalysis. *Proc. Natl. Acad. Sci. U. S. A.* **98**, 13649–13654
61. Morales-Ríos, E., De La Rosa-Morales, F., Mendoza-Hernández, G., Rodríguez-Zavala, J. S., Celis, H., Zarco-Zavala, M., *et al.* (2010) A novel 11-kDa inhibitory subunit in the F_1F_O ATP synthase of *Paracoccus denitrificans* and related α-proteobacteria. *FASEB J.* **24**, 599–608

62. Wong, C.-F., and Grüber, G. (2020) The unique C-terminal extension of mycobacterial F-ATP synthase subunit α is the major contributor to its latent ATP hydrolysis activity. *Antimicrob. Agents Chemother.* **64**, e01568-20
63. Sternweis, P. C., and Smith, J. B. (1980) Characterization of the inhibitory (ε) subunit of the proton-translocating adenosine triphosphatase from *Escherichia coli*. *Biochemistry* **19**, 526–531
64. Feniouk, B. A., Suzuki, T., and Yoshida, M. (2006) The role of subunit epsilon in the catalysis and regulation of F_OF_1-ATP synthase. *Biochim. Biophys. Acta* **1757**, 326–338
65. Guo, H., Courbon, G. M., Bueler, S. A., Mai, J., Liu, J., and Rubinstein, J. L. (2021) Structure of mycobacterial ATP synthase bound to the tuberculosis drug bedaquiline. *Nature* **589**, 143–147
66. Pullman, M. E., and Monroy, G. C. (1963) A naturally occurring inhibitor of mitochondrial adenosine triphosphatase. *J. Biol. Chem.* **238**, 3762–3769
67. Kobayashi, R., Ueno, H., Okazaki, K.-i., and Noji, H. (2023) Molecular mechanism on forcible ejection of ATPase inhibitory factor 1 from mitochondrial ATP synthase. *Nat. Commun.* **14**, 1682
68. Cabezón, E., Montgomery, M. G., Leslie, A. G. W., and Walker, J. E. (2003) The structure of bovine F_1-ATPase in complex with its regulatory protein IF_1. *Nat. Struct. Mol. Biol.* **10**, 744–750
69. Kane, P. M. (1995) Disassembly and reassembly of the yeast vacuolar H^+-ATPase *in vivo*. *J. Biol. Chem.* **270**, 17025–17032
70. Sumner, J.-P., Dow, J. A. T., Earley, F. G. P., Klein, U., Jäger, D., and Wieczorek, H. (1995) Regulation of plasma membrane V-ATPase activity by dissociation of peripheral subunits. *J. Biol. Chem.* **270**, 5649–5653